

# Electron-Deficiency Aromaticity in Silicon Nanoclusters

Holger Vach<sup>\*,†</sup>

<sup>†</sup>CNRS – LPICM, Ecole Polytechnique, 91128 Palaiseau, France

 Supporting Information

**ABSTRACT:** Aromaticity in silicon-containing molecules has been a controversy for more than a century. Combining molecular dynamics simulations with *ab initio* calculations, we show here that it is possible to obtain aromatic-like behavior with pure hydrogenated silicon clusters without the need for multiple bonds. To this end, we exploit the natural tendency of silicon toward overcoordination to construct electron-deficient molecules with ring structures. Even without the incorporation of any protective bulky substituents the resulting structures are more stable than any other known hydrogenated silicon nanoparticles of this size and exhibit aromatic-like properties due to strong electron delocalization.

## I. INTRODUCTION

As early as 1885, A. Polis explored the possibility of aromatic silicon compounds.<sup>1</sup> Despite this early work, the concept of aromaticity in silicon-containing molecules was largely discarded until West et al. realized a stable Si=Si double bond<sup>2</sup> in 1981 and Sekiguchi et al. a stable Si≡Si triple bond<sup>3</sup> in 2004. These breakthrough discoveries sparked a considerable interest in formally *sp*- and *sp*<sup>2</sup>-hybridized silicon atoms and in delocalized  $\pi$ -systems for silicon.<sup>4–11</sup> Because of the key role of benzene in the field of aromatic chemistry, the synthesis of a stable hexasilabenzene molecule has been considered as the “holy grail” in the quest for silicon aromaticity for a long time.<sup>12–14</sup> Recently, the observation of a tricyclic aromatic isomer of Si<sub>6</sub>R<sub>6</sub> with “R” being 2,4,6-triisopropylphenyl was reported that shows cyclic delocalization of six mobile electrons across the central four-membered ring.<sup>15</sup> While being much more bulky and complex than the benzene analogue, we should not forget that this strive for new and untypical molecules is not only an exciting experience in itself, but it is essential for improving our “understanding of that fundamental yet fuzzy entity—the chemical bond”.<sup>16</sup> To advance our comprehension yet further and as an alternative to current multiple-bond strategies, we present here a fundamentally novel approach to induce electron delocalization and, hence, aromatic-like behavior in silicon clusters. We like to term this new phenomenon “electron-deficiency aromaticity”, and we claim that it occurs more naturally for silicon than the conventional multiple bond aromaticity.

While both carbon and silicon are elements of the same column of the periodic table of elements, they behave strikingly differently when it comes to aromaticity. Conventional carbon aromaticity is based on a multiple bond concept; i.e. there are always more than two electrons between two adjacent carbon atoms. This principle perfectly suits hydrocarbons since carbon has a higher electronegativity than hydrogen and since carbon readily forms configurations with less than four neighbors; e.g. ethylene and acetylene. For silicon, however, exactly the contrary is true: it is less electronegative than hydrogen and it does in general not get involved in configurations where it has less than four neighbors and rather favors overcoordination.<sup>17–19</sup> In the same sense, both liquid carbon and liquid

silicon are metallic at ambient pressures, but liquid carbon is composed of 2-fold, 3-fold, and 4-fold coordinated atoms,<sup>20</sup> whereas silicon in the liquid state exhibits a typical coordination number of six to seven.<sup>21,22</sup> Such an overcoordination, however, leads to bonds that are poor in electrons.

Our present work is, therefore, based on the fundamental idea that in conventional carbon aromaticity there are in general too many electrons to be accommodated in only single bonds between all involved carbon atoms. For the silicon atoms of the overcoordination configurations presented here, on the contrary, there are not quite enough electrons for single bonds between all involved silicon atoms. In both cases, however, nature resolves this problem of having either too many or not quite enough electrons by delocalizing the participating electrons. As a consequence of this structure-induced electron delocalization, we have recently predicted the existence of overcoordinated hydrogenated silicon clusters with a magnetic shielding that exceeds the one of benzene and that are more stable than any other known silicon clusters.<sup>23</sup> Here, we will explore the origin of the unusual properties of those nanoparticles.

## II. EXAMPLES FOR OVERCOORDINATED HYDROGENATED SILICON ENTITIES

The most straightforward manner in constructing a monocyclic molecule in which silicon atoms are overcoordinated (i.e., having more than four closest neighbors) is to add a silicon atom in the center of the well-known and nonplanar cyclohexasilane Si<sub>6</sub>H<sub>12</sub> molecule.<sup>24</sup> Geometrical optimization leads to an armchair structure that is, indeed, more planar than the parent Si<sub>6</sub>H<sub>12</sub> molecule (see Figure 1a). While its magnetic shielding suggests possible aromatic behavior, a frequency analysis readily reveals that such a Si<sub>7</sub>H<sub>12</sub> structure cannot be stable. This instability is due to the fact that silicon is less electronegative than hydrogen; that is hydrogen atoms extract electrons out of adjacent silicon–silicon bonds, whereas they supply some of their electrons to carbon–carbon bonds due to the relatively high electronegativity of carbon. For the

Received: December 3, 2011

Published: May 11, 2012



ACS Publications

© 2012 American Chemical Society

2088

dx.doi.org/10.1021/ct2008704 | J. Chem. Theory Comput. 2012, 8, 2088–2094

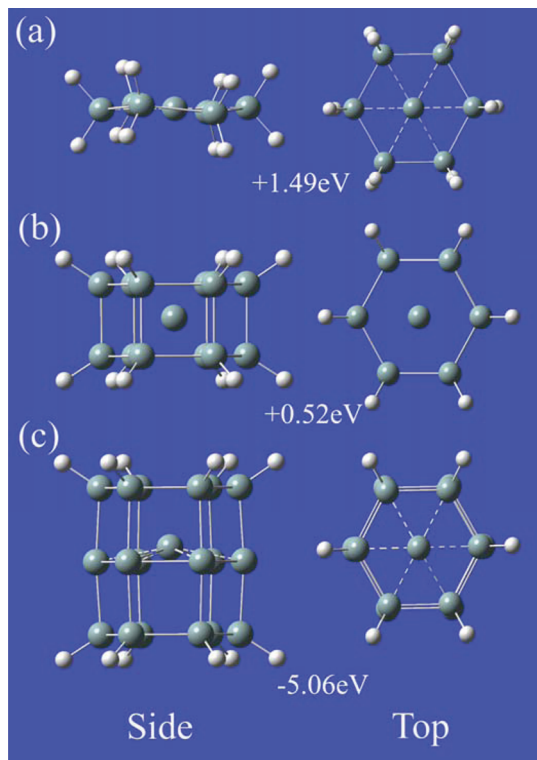


**Figure 1.** Examples of an unstable (a), metastable (b), and stable (c) overcoordinated hydrogenated silicon nanostructure. The given values correspond to the change in *ab initio* MP2 system energy for structures optimized at the MP2 level when a silicon atom is brought from an infinite distance to the center or close to the center of the corresponding empty structure.

hypothetical  $\text{Si}_7\text{H}_{12}$  of above, this electron extraction leads to severely electron-deficient bonds causing it to be unstable. Therefore, we explored as next possible overcoordination candidate a structure with relatively less hydrogen atoms; i.e. we introduced an additional silicon atom in the cage of the fullerene-like  $\text{Si}_{12}\text{H}_{12}$  molecule.<sup>25,26</sup> The resulting structure (see Figure 1b) is potentially stable since the frequency analysis as above shows no imaginary frequencies. To test thermal stability, we heated the optimized  $\text{Si}_{13}\text{H}_{12}$  structure slowly from zero Kelvin. While the structure seems to remain intact until about 200 K, the center silicon atom escapes from the fullerene-like cage within 150 fs at room temperature. Such a behavior does not come unexpectedly since the  $\text{Si}_{12}\text{H}_{12}$  fullerene actually loses about 0.5 eV in stability by the introduction of the additional center silicon atom. After its escape, this additional silicon atom rapidly transforms the structure shown in Figure 1b into an ill-defined isomer with a cohesive energy of about -3.2 eV which is quite comparable to the known cohesive energies for optimized silicon nanostructures of this size but with only four hydrogen atoms of about -3.8 eV.<sup>27,28</sup>

To reduce yet further the influence of hydrogen atoms, we added a third hydrogen-free silicon hexagon between the two hydrogenated ones of  $\text{Si}_{12}\text{H}_{12}$  to obtain a small  $\text{Si}_{18}\text{H}_{12}$  silicon nanotube which is the hexagonal analogue to the stable pentagonal  $\text{Si}_{15}\text{H}_{10}$  discussed in detail in ref 29. Before adding a central Si atom as above, we have optimized this new empty structure at different levels of theory, and we have assured that it is potentially stable (i.e., it does not exhibit any imaginary frequencies at any level of theory). The resulting optimized  $\text{Si}_{18}\text{H}_{12}$  structure has B3LYP and MP2 energies of -5218.49

hartree and -5211.64 hartree, respectively, which gives it about the same binding energy per atom as its pentagonal analogue of ref 29. In this nanotube, all silicon atoms are four-times coordinated. Upon introduction of an additional silicon atom close to the center, we obtain a MP2 optimized structure (see Figure 1c) that actually gains -5.06 eV in stability (see Computational Details below) which clearly exceeds not only the cohesive energy of comparable clusters,<sup>28</sup> but even the one of bulk silicon of -4.61 eV;<sup>30,31</sup> i.e., the binding is too strong to be understood in the framework of regular covalent silicon bonds. For this comparison with other clusters of the same size, we have calculated the cohesive energy resulting from the MP2 optimized structures of  $\text{Si}_{18}$  and  $\text{Si}_{19}$  to be -3.78 eV which agrees well with previously published values.<sup>28</sup> The structural details and atomic charges of the MP2 optimized  $\text{Si}_{19}\text{H}_{12}$  cluster can be found in the Supporting Information.

Using known cohesive energies for silicon and hydrogen,<sup>27,28,32</sup> we find actually that the proposed  $\text{Si}_{19}\text{H}_{12}$  structure exceeds the experimentally known  $\text{Si}_{29}\text{H}_{24}$  cluster<sup>33</sup> by more than 6 eV in stability. The  $\text{Si}_{19}\text{H}_{12}$  nanoparticle can be characterized by three parallel and perfectly planar hexagons with the center silicon atom slightly above the central hexagon plane (see Figure 1c). A frequency analysis confirms its vacuum stability since there are no imaginary frequencies. We have used molecular dynamics techniques to heat the structure slowly from 0 K to 1200 K. Even at these extreme conditions and despite the resulting large vibrational amplitudes, the  $\text{Si}_{19}\text{H}_{12}$  structure remains thermally stable. A typical 2 ps segment of the entire 10 ns trajectory can be viewed in the Supporting Information. In the following, we demonstrate that this unexpected stability can be traced back to an extremely strong electron delocalization mechanism resulting from the electron deficiency of the proposed structure.<sup>34</sup>

### III. STABILIZATION THROUGH ELECTRON DELOCALIZATION

For both hydrogenated external hexagons in  $\text{Si}_{19}\text{H}_{12}$  (see Figure 1c), a natural bond orbital (NBO) analysis<sup>35</sup> shows reasonably well localized  $\sigma_{\text{Si}-\text{Si}}$  and  $\sigma_{\text{Si}-\text{H}}$  natural bond orbitals (1.9490 and 1.9875 electrons, respectively). For the central silicon hexagon, however, severely depleted  $\sigma_{\text{Si}-\text{Si}}$  bonds (1.6440e) and corresponding high occupancy  $\sigma^*_{\text{Si}-\text{Si}}$  antibonds (0.1432e) are found. In contrast to the other bonds, the silicon–silicon bonds of the central hexagon exhibit a clear  $sp^2$  hybridization character. The bonds between two neighbor silicon atoms belonging respectively to an external and the central hexagon are less severely depleted (1.8445e); the corresponding  $\sigma_{\text{Si}-\text{Si}}$  bonds are formed from *p*-rich ( $sp^{4.5}$ ) hybrids on both Si atoms slightly polarized (about 58%) toward the Si atoms of the central hexagon. The two lone-pairs LP<sub>1</sub>(G) and LP<sub>2</sub>(G) of the center silicon atom “G” show strong depletion (1.7361e and 1.0280e, respectively) and *sp* hybridization. Both corresponding acceptor lone-pair orbitals LP<sub>3</sub>\*<sup>(G)</sup> and LP<sub>4</sub>\*<sup>(G)</sup> have pure *p*-character and are highly occupied (0.8609e). When actually adding up all those electrons that are “missing” in the bonds of the  $\text{Si}_{19}\text{H}_{12}$  structure, we find precisely 6 electrons that are thus available for delocalization. While this number does obey the (4*n*+2) Hückel’s rule, this coincidence has to be considered fortuitous since  $\text{Si}_{19}\text{H}_{12}$  is neither monocyclic nor two-dimensional.

The NBO analysis further confirms that  $\text{Si}_{19}\text{H}_{12}$  has a strongly delocalized structure with high stabilization energies “E(2)”. In Figure 2, we summarize the most important

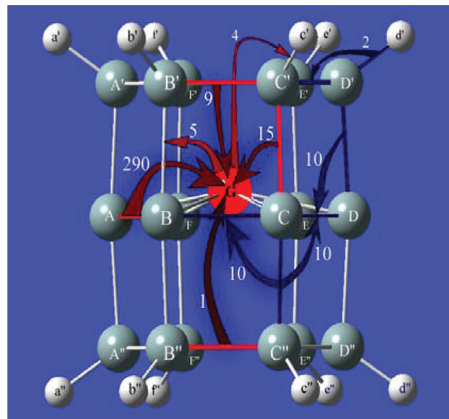


**Figure 2.** Some examples of E(2) stabilization energies resulting from delocalization between donor and acceptor sites. Energies are given in kcal/mol. Blue arrows show delocalization patterns between atomic bonds, while red arrows indicate delocalization from donor lone pairs LP(G) of the center silicon atom “G” to acceptor atomic bonds and from donor atomic bonds to acceptor lone pairs LP\*(G) of the center silicon atom.

delocalization patterns between atomic bonds (in blue) and between the lone pair electrons of the center silicon atom “G” and atomic bonds (in red). While a direct comparison of stabilization energies between two different molecules has only limited meaning, we just like to point out as a qualitative comparison that the corresponding stabilization energies for benzene obtained with the same method and level of theory are up to one order of magnitude smaller. These strong electron delocalization mechanisms are at the origin of the overall stabilization energy of about 5.06 eV shown in Figure 1c resulting from the insertion of the center silicon atom.

Whatever the origin of the delocalization toward the center silicon atom is, it leads to a population of the acceptor lone pair orbitals LP<sub>3</sub>\* (G) and LP<sub>4</sub>\* (G). In Figure 3, a display of the corresponding “Natural Localized Molecular Orbitals”<sup>36</sup> (NLMO) is shown. Superposition of the energetically degenerate LP<sub>3</sub>\* (G) and LP<sub>4</sub>\* (G) orbitals clearly illustrates the crucial role of these lone pair orbitals in promoting electron delocalization not only within the central hexagon plane but also between the three silicon hexagons. We also like to mention that the lone pairs of the central six-membered ring predominantly point outward to reduce their mutual repulsion with a significant portion inside the cage within the central hexagon plane which further stabilizes the entire structure.<sup>37</sup>

A unique feature of benzenoid systems is the cyclic pattern of conjugation allowing each localized  $\pi$  bond to delocalize into two adjacent  $\pi^*$  antibonds in concerted counter-rotating triple cycles. In the same manner, we find for the  $sp^2$  hybridized bonds in the central hexagon (see Figure 2 for atom referencing)

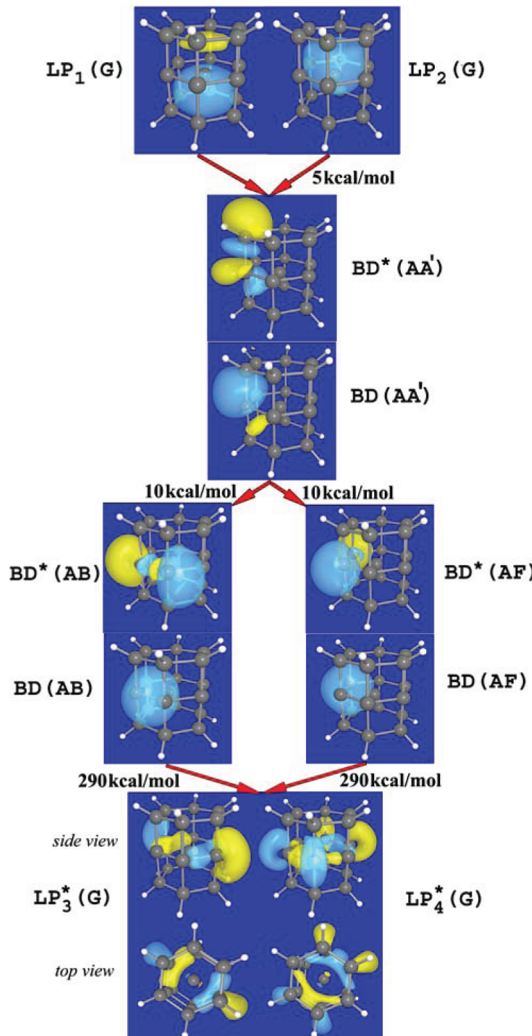
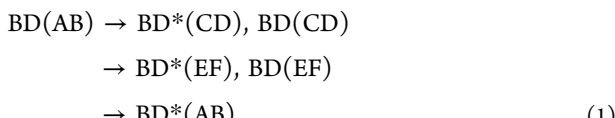
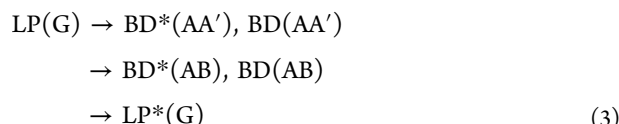
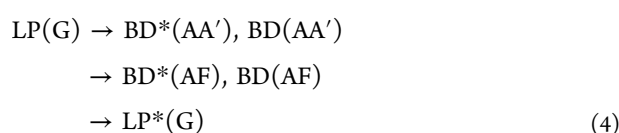


**Figure 3.** Delocalization patterns illustrating eqs 3 and 4. The most efficient delocalization pattern is illustrated that leads to the population of the energetically degenerate molecular orbitals LP<sub>3</sub>\* (G) and LP<sub>4</sub>\* (G). The numbers indicate the stabilization energies corresponding to each of the delocalization steps. Note that the same pattern is observed for each of the twelve bonds connecting the external hexagons to the central one (for atom referencing see Figure 2).

Each step of those cycles results in a stabilization energy of about 1.1 kcal/mol. In addition, we also find delocalization to the adjacent neighbors as  $\text{BD}(\text{AB}) \rightarrow \text{BD}^*(\text{BC})$ , etc. with a slightly higher stabilization energy of 1.8 kcal/mol. Both delocalization patterns are, however, quite negligible in comparison to those shown in Figure 2. The most efficient of those cyclic delocalization patterns is the one that “powers” the central hexagon

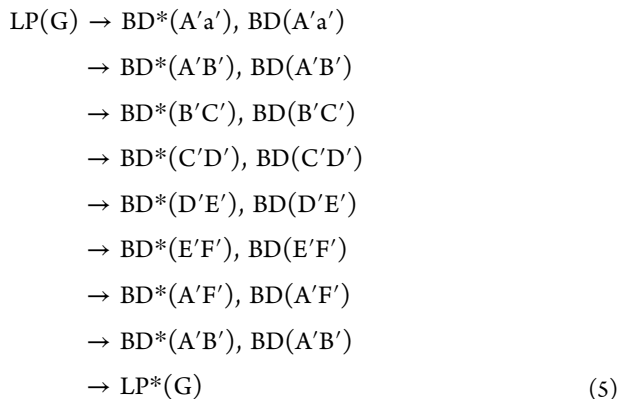


and simultaneously



(see Figure 3). In fact, we find this cyclic pattern for each of the twelve Si–Si bonds connecting the outer hexagons to the central one. Such concerted donor–acceptor interactions are inherently cooperative, so that each  $\text{BD} \rightarrow \text{BD}^*$  interaction of the filled  $\text{Si}_{19}\text{H}_{12}$  nanotube is strengthened relative to a corresponding interaction in the empty  $\text{Si}_{18}\text{H}_{12}$  nanotube.

There is no efficient delocalization route going directly from the center atom “G” to the silicon atoms of the outer hexagons. For the outer hexagon that is closer to the center silicon atom, the delocalization primarily transits via the silicon/hydrogen bonds



and simultaneously in the counter-rotating direction. Besides, there is also a direct delocalization path to  $\text{LP}^*(\text{G})$  from each horizontal bond, as for example from  $\text{BD}(\text{A}'\text{B}')$ . Again, the same delocalization mechanism takes place for all six Si–H bonds. For the other outer hexagon, the most efficient delocalization pathway goes again through the six vertical Si–Si bonds connecting this hexagon to the central one. The fact that the Si–H bonds are hardly involved for this hexagon leads to an electron cloud that is concentrated closer to the central longitudinal axis of the finite nanotube than for the other outer hexagon (see Figure 4). We also like to note that despite the absence of formal multiple bonds the overlap of occupied atomic orbitals often leads to maximum electron density distributions being located above and below the three hexagon planes similar to what is known for aromatic carbon

compounds;<sup>23</sup> see for example the “highest occupied molecular orbital” (HOMO) displayed in Figure 4.

Finally, we have to address the question how the center silicon atom “G” binds to the other silicon atoms. To this end, we have calculated the standard Wiberg bond index, the atom–atom overlap-weighted NAO bond order index, and the linear NLMO/NPA bond orders index<sup>36</sup> which are 3.551, 4.010, and 4.174, respectively. The corresponding atom–atom bond orders between the center silicon atom and its six neighbors in the central hexagon are 0.478, 0.553, and 0.605, respectively. These values strongly suggest a possible description as covalent “half-bonds” for the center silicon atom with its closest neighbors which strengthen our initial idea of an electron-deficient nanostructure.<sup>34</sup> An analysis of possible resonance structures strongly supports this interpretation: Each of the leading resonance structures corresponds to a configuration where the center silicon atom connects with one bond to one of the surrounding silicon atoms: the closer this atom is, the higher is the weight of that resonance structure. Some of the resonance structures show as many as six simultaneous bonds with the closest neighbors. Such structures, however, have a much lower weight. These observations can simply be summarized in the picture that the electrons are highly delocalized between the center atom and its neighbors.

#### IV. MAGNETIC SHIELDING

One manifestation of this significant electron delocalization is the aromatic-like behavior of the proposed structures leading to their unusual stability, the bond length equalization, and some characteristic spectroscopic features.<sup>23</sup> Since aromaticity is related to induced ring currents, magnetic properties are particularly important for its detection and evaluation. Among several indexes nucleus-independent chemical shifts (NICS)<sup>38</sup> have become the most widely used aromaticity probe due to its simplicity and efficiency.<sup>39</sup>

In Figure 5, we display the NICS values for the proposed  $\text{Si}_{19}\text{H}_{12}$  cluster evaluated in two perpendicular directions. Since  $\sigma$  contributions usually fall off faster than  $\pi$  ones normal to a ring, we show in Figure 5(a) a scan of NICS values determined along the longitudinal direction in the center of the nanoparticle. As can be seen, the shielding never drops below the maximum values of benzene over the entire length inside of the finite nanotube. Even outside of the nanotube, the shielding diminishes surprisingly slowly leading to NICS(1) values of  $-7.1$  ppm and  $-9.4$  ppm at a distance of  $1\text{ \AA}$  below (see Figure 5b) and above (see Figure 5d) the external hexagons of the finite nanotube, respectively. In the orthogonal direction, each of the three hexagons exhibits a magnetic shielding that also largely exceeds the one of benzene which is coherent with the extremely high stabilization energy of about  $5.1$  eV. As for benzene, the shielding has a local minimum in the center of both external hexagons which can be understood by the fact that the principal delocalization routes pass through the twelve bonds connecting the external hexagons to the central one (see Figure 3).

#### V. COMPUTATIONAL DETAILS

All geometrical and electronic structure optimizations were systematically performed with both density functional theory using the hybrid, nonlocal exchange, and correlation functional of Becke, Lee, Parr, and Yang (B3LYP) and *ab initio* Møller–Plesset second order perturbation theory (MP2) calculations

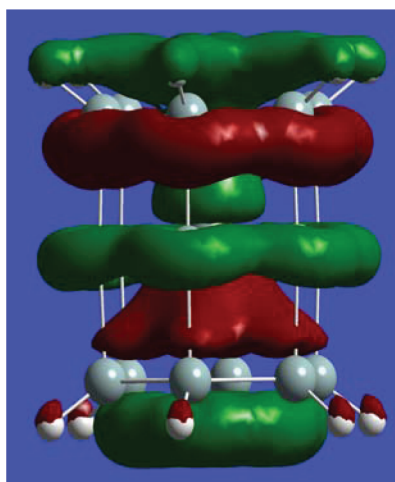


**Figure 4.** Isovalue contour plots of the highest-occupied molecular orbital (HOMO) representing the electron density obtained at the B3LYP/6-311++G\*\* level with an isovalue of  $0.02\text{ e}/\text{\AA}^3$  for the  $\text{Si}_{19}\text{H}_{12}$  cluster.

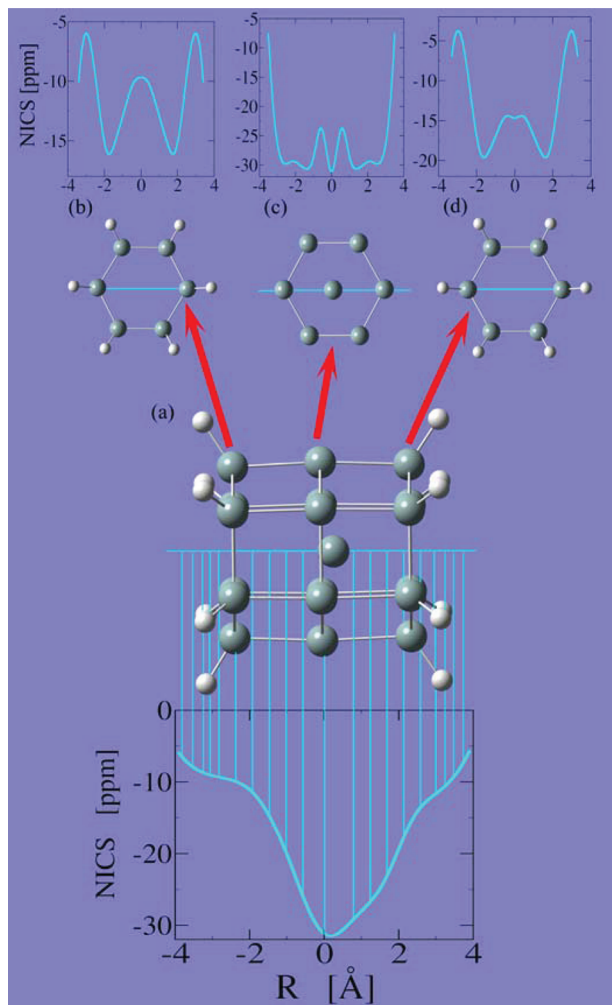


**Figure 5.** Longitudinal and perpendicular NICS values: (a) the magnetic shielding has been evaluated along the turquoise horizontal line in the longitudinal direction in the center of the finite nanotube; (b), (c), and (d) the NICS values have been determined within each of the three hexagonal planes along the turquoise lines underneath the center silicon and underneath or above the hydrogen atoms.

always using both the split-valence triple- $\zeta$  Pople-type and the Dunning-type basis sets with diffuse and polarization functions for both silicon and hydrogen atoms using Gaussian09.<sup>40,41</sup> As expected for well-known hydrogenated silicon systems, the B3LYP and the MP2 computations also lead to the same results for the clusters presented here. We have used open shell systems to optimize the structures for different multiplicities and found that the lowest energy structure of  $\text{Si}_{19}\text{H}_{12}$  is obtained for the singlet state that can well be described as a closed shell system. In all cases, a frequency analysis was performed to verify vacuum stability. Optimization with the plane-wave code VASP-4.6.35 systematically leads to the same results as those presented here.<sup>42,43</sup>

Since the B3LYP functional is known to significantly underestimate atomization energies in electron-deficient structures,<sup>44</sup> we have calculated the cohesive energy resulting from the introduction of the center Si atom for  $\text{Si}_{19}\text{H}_{12}$  in five different ways with the above basis sets: two DFT calculations using respectively the M06 [refs 45 and 46] and the Perdew-Burke-Enzerhof (PBE)<sup>47</sup> exchange–correlation functional with an energy cutoff of 500 eV and all-electron plane-wave basis

sets within the projector augmented wave (PAW) method<sup>48</sup> and three basis-set-superposition-error (BSSE) corrected MP2 calculations considering Frozen-core (FC) MP2 energies of FC-MP2 optimized structures; single point calculations (SPC) of Full-MP2 energies of B3LYP optimized structures; and finally, Full-MP2 energies of Full-MP2 optimized structures yielding an average stabilization energy of  $(5.1 \pm 0.3)$  eV.

For the molecular dynamics simulations, we have employed a Born–Oppenheimer approach (BOMD); first using the VENUS program<sup>49</sup> with the semiempirical PM3 method for long-time simulations, up to 10 ns with a time step of 0.01 fs to test for thermal stability. Then, all of those simulations were confirmed with the *ab initio* molecular dynamics code VASP<sup>42,43</sup> on a shorter time scale, up to 100 ps with a time step of 0.1 fs and a cutoff energy of 500 eV. For the present system, both MD approaches lead to nearly identical results which is not surprising since the stabilization energy resulting from the introduction of the additional silicon atom in the empty  $\text{Si}_{18}\text{H}_{12}$  nanotube calculated with VENUS on the semiempirical PM3 level is  $-4.60$  eV, while the VASP program with PAW-PBE and a conjugate-gradient optimizer yields a quite comparable energy of  $-4.73$  eV. Typically, the total energy is conserved to better than  $3 \times 10^{-9}$  per step for all MD simulations. The heating of the clusters was achieved with a Nosé-thermostat.

## VI. SUMMARY AND CONCLUSIONS

Although aromaticity was initially only confined to planar hydrocarbon molecules with delocalized  $\pi$  electrons, this concept has nowadays evolved to three-dimensional systems,<sup>50,51</sup> to other elements,<sup>52–55</sup> to  $\sigma$ -aromaticity,<sup>56–62</sup> to stable unsaturated silicon clusters,<sup>63–67</sup> and even to the delocalization of transition metal d-electrons.<sup>68–70</sup> In the present work, we propose to extend the aromaticity concept yet further by exploiting the electron-deficiency of a system to induce electron delocalization and, thus, enhanced stability. As a concrete example, we scrutinized here the case of over-coordinated hydrogenated silicon clusters with ring structure geometries. Those proposed nanoparticles might perhaps not be as robust as benzene or possible molecules involving double or triple silicon bonds, but we predict them to remain thermally stable at temperatures exceeding 1000 K. We showed that their properties perfectly comply with those expected for aromatic substances: first, all three hexagons are perfectly planar; second, all silicon–silicon bonds in each of the three hexagons are equivalent in length; third, the introduction of the center silicon atom increases the stability by more than the cohesive energy of bulk silicon which cannot be understood on the basis of regular covalent bonds in silicon and which makes them more stable than the experimentally known  $\text{Si}_{29}\text{H}_{24}$  nanoparticle; fourth, they manifest outstanding spectroscopic properties; fifth, there are six electrons being delocalized and finally, their magnetic shielding exceeds the one of benzene. Because of the absence of formal multiple bonds, we define the here observed “electron-deficiency aromaticity” as a chemical property in which the addition of one atom to an already saturated ring structure causes an increase of stability that exceeds the corresponding cohesive energy as a result of the induced electron delocalization.

The strongly delocalized nature of their electronic structure does not only increase somewhat the stability of the proposed clusters, but it is at the origin of their very existence. Therefore, their resulting mechanical, chemical, electronic, and optical

properties are so unique that they will open up new avenues in various emerging nanotechnological domains. Finally, the proposed new concept of electron-deficiency aromaticity is not necessarily restricted to silicon but might readily be extended to other chemical elements also showing a tendency to overcoordination.

## ■ ASSOCIATED CONTENT

### Supporting Information

Cartesian coordinates for all structures discussed in Figure 1; two additional figures showing radial distribution functions for five different temperatures and atomic charges for Si<sub>19</sub>H<sub>12</sub>; a short film showing a typical 2 ps segment of the 10 ns trajectory at 1200 K. This material is available free of charge via the Internet at <http://pubs.acs.org>.

## ■ AUTHOR INFORMATION

### Corresponding Author

\*E-mail: holger.vach@polytechnique.edu.

### Notes

The authors declare no competing financial interest.

## ■ ACKNOWLEDGMENTS

We like to express our sincere gratitude to Pascal Le Floch, Gilles Ohanessian, Ann English, Gilles Peslherbe, and Qadir Timerghazin for their precious help at different stages of the present work. The calculations were performed using HPC resources from GENCI-IDRIS (Grant 2009-0910642).

## ■ REFERENCES

- (1) Polis, A. *Ber. Dtsch. Chem. Ges.* **1885**, *18*, 1540–1544.
- (2) West, R.; Fink, M. J.; Michl, J. *Science* **1981**, *214*, 1343–1344.
- (3) Sekiguchi, A.; Kinjo, R.; Ichinohe, M. *Science* **2004**, *305*, 1755–1757.
- (4) Scheschkewitz, D. *Angew. Chem., Int. Ed.* **2011**, *50*, 3118–3119.
- (5) Lee, V. Y.; Sekiguchi, A. *Angew. Chem., Int. Ed.* **2007**, *46*, 6596–6620.
- (6) Wakita, K.; Tokitoh, N.; Okazaki, R.; Nagase, S. *Angew. Chem., Int. Ed.* **2000**, *39*, 634–636.
- (7) Kinjo, R.; Ichinohe, M.; Sekiguchi, A.; Takagi, N.; Sumimoto, M.; Nagase, S. *J. Am. Chem. Soc.* **2007**, *129*, 7766–7767.
- (8) Ichinohe, M.; Igarashi, M.; Sanuki, K.; Sekiguchi, A. *J. Am. Chem. Soc.* **2005**, *127*, 9978–9979.
- (9) Lee, V. Y.; Takanashi, K.; Matsuno, T.; Ichinohe, M.; Sekiguchi, A. *J. Am. Chem. Soc.* **2004**, *126*, 4758–4759.
- (10) Abe, T.; Iwamoto, T.; Kira, M. *J. Am. Chem. Soc.* **2010**, *132*, 5008–5009.
- (11) Dewar, M. J. S.; Lo, D. H.; Ramsden, C. H. *J. Am. Chem. Soc.* **1975**, *97*, 1311–1318.
- (12) Nagase, S.; Teramae, H.; Kudo, T. *J. Chem. Phys.* **1987**, *86*, 4513–4517.
- (13) Baldridge, K. K.; Uzan, O.; Martin, J. M. L. *Organometallics* **2000**, *19*, 1477–1487.
- (14) Sekiguchi, A.; Yatabe, T.; Kabuto, C.; Sakurai, H. *J. Am. Chem. Soc.* **1993**, *115*, 5853–5854.
- (15) Abersfelder, K.; White, A. J. P.; Rzepa, H. S.; Scheschkewitz, D. *Science* **2010**, *327*, 564–566.
- (16) Hoffmann, R.; Hopf, H. *Angew. Chem., Int. Ed.* **2008**, *47*, 4474–4481.
- (17) McMillan, P. F.; Wilson, M.; Daisenberger, D.; Machon, D. *Nat. Chem.* **2005**, *4*, 680–684.
- (18) Sastry, S.; Angell, C. A. *Nat. Chem.* **2003**, *2*, 739–743.
- (19) Deb, S. K.; Wilding, M. C.; Somayazulu, M.; McMillan, P. F. *Nature* **2001**, *414*, 528–530.
- (20) Galli, G.; Martin, R. M.; Car, R.; Parrinello, M. *Phys. Rev. Lett.* **1989**, *63*, 988–991.
- (21) Jank, W.; Hafner, J. *Phys. Rev. B* **1990**, *41*, 1497–1515.
- (22) Jakse, N.; Krishnan, S.; Artacho, E.; Key, T.; Hennet, L.; Glorieux, B.; Pasturel, A.; Price, D. L.; Saboungi, M.-L. *Appl. Phys. Lett.* **2003**, *83*, 4734–4736.
- (23) Vach, H. *Nano Lett.* **2011**, *11*, 5477–5481.
- (24) Hengge, E.; Kovar, D. *Angew. Chem., Int. Ed.* **1977**, *16*, 403–404.
- (25) Earley, C. W. *J. Phys. Chem. A* **2000**, *104*, 6622–6627.
- (26) Naruse, Y.; Inagaki, S. In *Current Chemistry*; Inagaki, S., Ed.; Springer Verlag: 2009; Vol. 289, pp 265–291.
- (27) Meloni, G.; Gingerich, K. A. *J. Chem. Phys.* **2001**, *115*, 5470–5476.
- (28) Singh, R. *J. Phys.: Condens. Matter* **2008**, *20*, 045226–1–14.
- (29) Bai, J.; Zeng, X. C.; Tanaka, H.; Zeng, J. Y. *Proc. Natl. Acad. Sci. U.S.A.* **2004**, *101*, 2664–2668.
- (30) Farid, B.; Godby, R. W. *Phys. Rev. B* **1991**, *43*, 14248–14250.
- (31) Paier, J.; Marsman, M.; Kresse, G. *J. Chem. Phys.* **2007**, *127*, 024103–1–024103–10.
- (32) Jing, Z.; Whitten, J. L. *Phys. Rev. B* **1992**, *46*, 9544–9550.
- (33) Rao, S.; Mantey, K.; Therrien, J.; Smith, A.; Nayfeh, M. *Phys. Rev. B* **2007**, *76*, 155316–1–9.
- (34) Pauling, L. *The Nature of the Chemical Bond*; Cornell University Press: 1960; p 363ff.
- (35) Reed, A. E.; Curtiss, L. A.; Weinhold, F. *Chem. Rev.* **1988**, *88*, 899–926.
- (36) Weinhold, F. Natural Bond Orbital Methods. In *Encyclopedia of Computational Chemistry*; Schleyer, P. v. R., Allinger, N. L., Clark, T., Gasteiger, J., Kollman, P. A., Schaefer III, H. F., Schreiner, P. R., Eds.; John Wiley & Sons: Chichester, UK, 1998; Vol. 3, pp 1792–1811.
- (37) Li, Z.-H.; Moran, D.; Fan, K.-N.; Schleyer, P. v. R. *J. Phys. Chem. A* **2005**, *109*, 3711–3716.
- (38) Schleyer, P. v. R.; Maerker, C.; Dransfeld, A.; Jiao, H.; Hommes, N. J. R. v. E. *J. Am. Chem. Soc.* **1996**, *118*, 6317–6318.
- (39) Chen, Z.; Wannere, C. S.; Corminboeuf, C.; Puchta, R.; Schleyer, P. v. R. *Chem. Rev.* **2005**, *105*, 3842–3888.
- (40) Frisch, M. J.; Trucks, G. W.; Schlegel, H. B.; Scuseria, G. E.; Robb, M. A.; Cheeseman, J. R.; Scalmani, G.; Barone, V.; Mennucci, B.; Petersson, G. A.; Nakatsuji, H.; Caricato, M.; Li, X.; Hratchian, H. P.; Izmaylov, A. F.; Bloino, J.; Zheng, G.; Sonnenberg, J. L.; Hada, M.; Ehara, M.; Toyota, K.; Fukuda, R.; Hasegawa, J.; Ishida, M.; Nakajima, T.; Honda, Y.; Kitao, O.; Nakai, H.; Vreven, T.; Montgomery, J. A., Jr.; Peralta, J. E.; Ogliaro, F.; Bearpark, M.; Heyd, J. J.; Brothers, E.; Kudin, K. N.; Staroverov, V. N.; Kobayashi, R.; Normand, J.; Raghavachari, K.; Rendell, A.; Burant, J. C.; Iyengar, S. S.; Tomasi, J.; Cossi, M.; Rega, N.; Millam, N. J.; Klene, M.; Knox, J. E.; Cross, J. B.; Bakken, V.; Adamo, C.; Jaramillo, J.; Gomperts, R.; Stratmann, R. E.; Yazyev, O.; Austin, A. J.; Cammi, R.; Pomelli, C.; Ochterski, J. W.; Martin, R. L.; Morokuma, K.; Zakrzewski, V. G.; Voth, G. A.; Salvador, P.; Dannenberg, J. J.; Dapprich, S.; Daniels, A. D.; Farkas, O.; Foresman, J. B.; Ortiz, J. V.; Cioslowski, J.; Fox, D. J. *Gaussian 09, Revision A.2*; Gaussian, Inc.: Wallingford, CT, 2009.
- (41) Stephens, P. J.; Devlin, F. J.; Chabalowski, C. F.; Frisch, M. J. *J. Phys. Chem.* **1994**, *98*, 11623–11627.
- (42) Kresse, G.; Hafner, J. *Phys. Rev. B* **1994**, *49*, 14251–14269.
- (43) Kresse, G.; Joubert, D. *Phys. Rev. B* **1999**, *59*, 1758–1775.
- (44) Paier, J.; Marsman, M.; Kresse, G. *J. Chem. Phys.* **2007**, *127*, 024103–1–10.
- (45) Zhao, Y.; Truhlar, D. G. *J. Chem. Phys.* **2006**, *125*, 194101–1–18.
- (46) Zhao, Y.; Truhlar, D. G. *Theor. Chem. Acc.* **2008**, *120*, 215–241.
- (47) Perdew, J. P.; Burke, K.; Ernzerhof, M. *Phys. Rev. Lett.* **1996**, *77*, 3865–3868.
- (48) Blöchl, P. E. *Phys. Rev. B* **1994**, *50*, 17953–17979.
- (49) Hase, W. L.; Duchovic, R. J.; Hu, X.; Lim, K. F.; Lu, D.-H.; Peslherbe, G. H.; Swamy, K. N.; Vander Linde, S. R.; Wang, H.; Wolf, R. J. VENUS96: General Chemical Dynamics Computer Program, Department of Chemistry - Wayne State University, Detroit, MI, 1996.

- (50) Osawa, E. *Philos. Trans. R. Soc. London, Ser. A* **1993**, *343*, 1–8.
- (51) Curl, R. E.; Smalley, R. E.; Kroto, H. W.; O'Brien, S.; Heath, J. *R. J. Mol. Graphics Modell.* **2001**, *19*, 185–186.
- (52) Huang, W.; et al. *Nat. Chem.* **2010**, *2*, 202–206.
- (53) Boldyrev, A. I.; Wang, L. S. *Chem. Rev.* **2005**, *105*, 3716–3757.
- (54) Islas, R.; Heine, T.; Merino, G. *J. Chem. Theory Comput.* **2007**, *3*, 775–781.
- (55) Tai, T. B.; Nguyen, M. T. *J. Chem. Theory Comput.* **2011**, *7*, 1119–1130.
- (56) Dewar, M. J. S. *Bul. Soc. Chim. Belg.* **1979**, *88*, 957–967.
- (57) Dewar, M. J. S.; McKee, M. L. *Pure Appl. Chem.* **1980**, *52*, 1431–1441.
- (58) Dewar, M. J. S. *J. Am. Chem. Soc.* **1984**, *106*, 669–682.
- (59) Cremer, D.; Kraka, E. *J. Am. Chem. Soc.* **1985**, *107*, 3800–3810.
- (60) Cremer, D.; Kraka, E. *J. Am. Chem. Soc.* **1989**, *111*, 3811–3819.
- (61) Sauers, P. R. *Tetrahedron* **1998**, *54*, 337–348.
- (62) Exner, K.; Schleyer, P. v. R. *J. Phys. Chem A* **2001**, *105*, 3407–3416.
- (63) Scheschkeitz, D. *Angew. Chem., Int. Ed.* **2005**, *44*, 2954–2956.
- (64) Abersfelder, K.; White, A. J. P.; Berger, R. J. F.; Rzepa, H. S.; Scheschkeitz, D. *Angew. Chem., Int. Ed.* **2011**, *50*, 7936–7939.
- (65) Fischer, G.; Huch, V.; Mayer, P.; Vasisht, S. K.; Veith, M.; Wiberg, N. *Angew. Chem., Int. Ed.* **2005**, *44*, 7884–7887.
- (66) Nied, D.; Köppe, R.; Klopper, W.; Schnöckel, H.; Breher, F. *J. Am. Chem. Soc.* **2010**, *132*, 10264–10265.
- (67) Berger, R. J. F.; Rzepa, H. S.; Scheschkeitz, D. *Angew. Chem., Int. Ed.* **2010**, *49*, 10006–10009.
- (68) Wannere, C. S.; Corminboeuf, C.; Wang, Z. X.; Wodrich, M. D.; King, R. B.; Schleyer, P. v. R. *J. Am. Chem. Soc.* **2005**, *127*, 5701–5705.
- (69) Tsipis, A. C.; Tsipis, C. A. *J. Am. Chem. Soc.* **2003**, *125*, 1136–1137.
- (70) Tsipis, C. A.; Karagiannis, E. E.; Kladou, P. F.; Tsipis, A. C. *J. Am. Chem. Soc.* **2004**, *126*, 12916–12929.